RSC Advances



This is an *Accepted Manuscript*, which has been through the Royal Society of Chemistry peer review process and has been accepted for publication.

Accepted Manuscripts are published online shortly after acceptance, before technical editing, formatting and proof reading. Using this free service, authors can make their results available to the community, in citable form, before we publish the edited article. This Accepted Manuscript will be replaced by the edited, formatted and paginated article as soon as this is available.

You can find more information about *Accepted Manuscripts* in the **Information for Authors**.

Please note that technical editing may introduce minor changes to the text and/or graphics, which may alter content. The journal's standard <u>Terms & Conditions</u> and the <u>Ethical guidelines</u> still apply. In no event shall the Royal Society of Chemistry be held responsible for any errors or omissions in this *Accepted Manuscript* or any consequences arising from the use of any information it contains.





Journal Name

ARTICLE

Received 00th January 20xx, Accepted 00th January 20xx

DOI: 10.1039/x0xx00000x

www.rsc.org/

Self-assembly of three shapes of anatase TiO₂ nanocrystals into horizontal and vertical two-dimensional superlattices

Yong Zhang, Fa-Min Liu*

Abstract: The bone-cuboid, spindle and rhombic TiO_2 nanocrystals have been achieved by a simple solvothermal method with the oleic acid and oleylamine volume ratio at 5/5, 4/6 and 3/7, respectively. X-ray diffraction (XRD) and selected area electron diffraction (SAED) results show that all of the three shapes of TiO_2 nanocrystals are highly crystallized anatase. Furthermore, for the first time, horizontal and vertical two-dimensional superlattices have been self-assembled with all three shapes of TiO_2 nanocrystals by controlling the amount of TiO_2 nanocrystals solution and the oleic acid. The self-assembly process is primarily driven by maximization of the packing density and tuning entropic depletion attraction forces. In addition, the nanodots, nanorods and nanospheres of TiO_2 nanocrystals have been obtained with various amount of H_2O_2 (0 ml, 0.05 ml, and 0.25 ml). These ordered two-dimensional superlattices may be suitable for the fabrication of functional ultrathin films which take full advantage of the directional and shape-dependent properties for wide ranging devices.

Keywords: titania nanocrystals, shape-controlled, self-assembly, supperlattices.

1 Introduction

Titanium dioxide nanocrystals (TiO₂ NCs) have attracted tremendous attention due to their potential applications in many fields such as catalysis, photovoltaic cell, electron field emission and sensors. 1-5 These applications arise from the unique chemical and physical properties of TiO₂ NCs, which depend on both the particle size, the crystal phase and the particle shape, even surface structure. 6-10 Controlling the shapes and sizes of TiO2 NCs is vital important in the fabrication of nanomaterials with desired properties. The solvothermal technique is widely used to tailor the high energy facets owing to its versatile ability in controlling the nucleation and growth behaviors of nanoparticles. Surface energies of different surfaces of TiO₂ NCs can be decreased effectively by the selective adsorption of appropriate inorganic ions or organic molecules as surfactants, so that the growth rates along specific orientations can be controlled. 11-14 For instance, Chen et al. 15 used sodium fluoride as the shape control agent to prepare highly crystalline TiO2 NCs enclosed by {101} and {001} facets via a simple microemulsion method. Similarly, the exploration of effective shape control agent for simple, economical, and green synthesis of homogeneous TiO2 NCs is still highly desirable. In addition, uniform TiO₂ NCs with different shapes can act as building blocks to form ordered

Department of Physics, School of Physics and Nuclear Energy Engineering, Beihang University, Beijing 100191, China. E-mail: fmliu@buaa.edu.cn; Tel:+86 -10-82338602. superlattices through self-assembly process.

Self-assembly of colloidal nanocrystals into ordered superlattices is emerging as a bottom-up approach to design and fabricate novel functional materials with tailored physical and chemical properties, which are promising for wide ranging devices, such as lasers, solar cells, photodetectors and LEDs. 16-²⁰ The collective properties of the superlattices can be determined not only by the intrinsic characteristics of the building blocks, but also by the synergistic interactions among the building blocks. Therefore, these collective properties can be engineered by the selection of the colloidal nanocrystals (with different size, shape, surface), as well as spatial symmetry of the resulting self-organized superlattice. 21-23 Although great advances have been achieved recently for the self-assembly of colloidal nanoparticle, $^{\mathbf{23-26}}$ only a few studies have been reported on the self-assembly of TiO2 NCs. Wang and co-workers obtained several ordered superlattices of anatase TiO₂ nanorods,²⁷ but how to achieve TiO₂ NCs with different shapes into anisotropic superlattices remains a great challenge.

In this paper, a facile solvothermal technique is performed to fabricate TiO $_2$ NCs with different shapes 28 , which combines oleylamine (OM) and oleic acid (OA) as two distinct capping ligands. The key feature of our approach is to use H_2O_2 as hydrolysis agent instead of H_2O vapor, because the H_2O_2 can easily react with titanium butoxide (TB) to form stable complex precursors. However, TB may react with H_2O to produce unstable hydroxyalkoxides at room temperature. Bone-cuboid, spindle and rhombic TiO $_2$ NCs are obtained with the OA/OM volume ratio at 5/5, 4/6 and 3/7, respectively. Subsequently, for the first time, the three shapes of TiO $_2$ NCs were all self-

ARTICLE Journal Name

assembled into horizontal and vertical two-dimensional (2D) superlattices by the liquid-air interface method. Finally, we analyzed these assemblies' structures and investigated several parameters that affecting the packing behaviors of the TiO_2 NCs. The self-assembly process is primarily driven by the packing density and the entropic depletion attraction forces. It is also found that TiO_2 NCs with a small truncation play a vital role in controlling the resulting superlattices. Moreover, the nanodots, nanorods and nanospheres of TiO_2 NCs have been obtained by changing the amount of H_2O_2 . Our study shows that the reported procedure may provide a simple and effective method for fabricating uniform anisotropic TiO_2 nanoparticles and their ordered superlattices with different packing structures.

2 Experimental

2.1 Synthesis of TiO₂ nanocrystals

All the reagents were purchased form Aladdin Industrial Corporation and used as received. The TiO₂ nanoparticles were synthesized according to a modified previous report.²⁸ In a typical synthesis, 1 ml of titanium butoxide (TB), 5 ml of oleic acid (OA), 5 ml of oleylamine (OM), 5 ml of absolute ethanol and 0.1 ml of hydrogen peroxide solution (H2O2, 30 wt.% in H₂O) were mixed together under stirring at room temperature for 15 min. The light yellow solution was transferred into a teflon-lined stainless steel autoclave and heated at 1802 for 12 h. The obtained white precipitates were washed several times with ethanol and then were dispersed in 30 ml hexane for the following self-assembled process. The bone-cuboid, spindle and rhombic TiO₂ nanoparticles were obtained with the OA/OM volume ratio at 5/5, 4/6 and 3/7 respectively. The morphology changes of bone-cuboid TiO2 nanoparticles were further investigated with various amount of H2O2 (0 ml, 0.05 ml, 0.15 ml and 0.25 ml).

2.2 Self-assembly of TiO₂ nanocrystals into superlattices

The two-dimensional superlattices were obtained by the liquid-air interface method. ²⁹ Firstly, 200 μ l, 400 μ l and 600 μ l solution (from 30 ml hexane) and certain amount of OA (0 μ l, 5 μ l, 10 μ l) were mixed, respectively. Then the mixed solutions were all diluted to 1 ml with hexane. Secondly, 200 μ l of each diluted solution was drop-casted on a dense liquid surface (ethylene glycol) in a sealed vail. The hexane slowly evaporated at room temperature, forming a continuous membrane at the liquid-air interface. Then the membranes were transferred to a TEM-grid and the grid was dried in vacuum prior to further investigation. For simplicity, the self-assembled TiO₂ NCs samples will be referred to as (200 μ l, 5 μ l), which means 200 μ l TiO₂ stock solution and 5 μ l OA in the final diluted solution.

2.3 Characterization

Powder X-ray diffraction (XRD) patterns were collected on a PANalytical X'Pert X-ray powder diffractometer equipped with a Cu K α 1 radiation source (λ =0.15406nm). Transmission

electron microscope (TEM) images and selected area electron diffraction (SAED) of ${\rm TiO_2}$ nanoparticles were obtained on a transmission electron microscope (TEM, JEOL-1011). The structures of the nanocrystals were measured by high-resolution transmission electron microscope (HRTEM, JEM-2011F).

3 Results and discussion

3.1 Synthesis of TiO₂ nanocrystals with different OA/OM ratios

Fig. 1 shows the TEM images of the TiO₂ nanoparticles (NPs) synthesized by varying the OA/OM volume ratio (here $H_2O_2=0.1$ ml). When the OA/OM volume ratio is 5/5, bonecuboid TiO₂ NPs with uniform morphology are obtained (Fig. 1a). By decreasing the OA/OM volume ratio to 4/6, monodisperse large spindle TiO₂ nanoparticles are produced (Fig. 1c). When decreasing this ratio to 3/7, the typical rhombic nanocrystals are prepared and TEM image reveals that the synthesized nanoparticles have a width of 13 nm and a length of 30 nm (Fig. 1e). To better visualize the crystal structure and the morphology of the obtained TiO2 NPs in detail, we characterized the products by HRTEM. In Fig. 1b, 1d and 1f, the lattice fringes with the spacing of about 0.34 nm and 0.48 nm correspond to the {101} planes and {001} planes of anatase respectively, and the interfacial angles are all about 68.3°, which is consistent with the theoretical value. On the basis of our HRTEM observations and the Wulff construction, 30 we propose that the morphology of bone-cuboid nanoparticles are mainly of {001} facets and {100} facets, while spindle nanoparticles are dominated by {101} facets and a part of {001} facets, and rhombic nanoparticles are mostly exposed with eight {101} lateral facets.

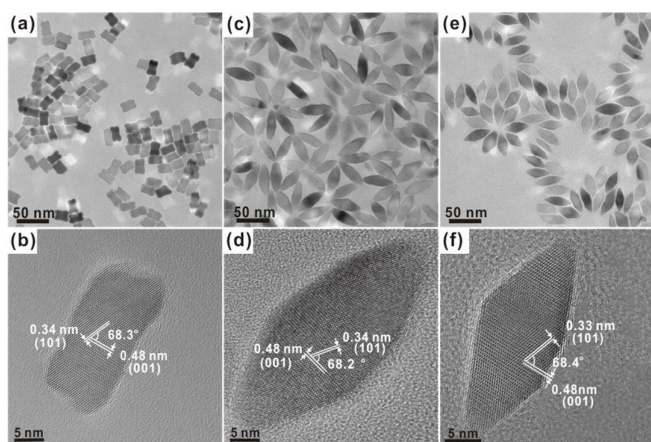


Fig. 1 TEM images of the TiO_2 nanoparticles (here H_2O_2 =0.1ml): (a) bone-cuboid; (c) spindle; (e) rhombic. HRTEM images of the TiO_2 nanoparticles: (b) bone-cuboid; (d) spindle; (f) rhombic.

The crystallinity of the obtained products was verified by powder X-ray diffraction (XRD). As shown in Fig. 2a, the typical XRD patterns of TiO_2 nanoparticles with (A) bone-cuboid, (B) spindle, and (C) rhombic shapes all show well-defined peaks

Journal Name ARTICLE

assigned to the single anatase phase (JCPDS No. 211272), indicating of the high crystallinity of these products. The (004) diffraction peaks of these products synthesized under different OA/OM ratio all appear more pronounced and sharper, compared to the bulk reference or nanospheres, suggesting the evolution along the preferential [001] crystallographic orientation. The intensity of the (200) peak and the (004) peak are always independent and correspond to a-axis and c-axis respectively.31 In addition, The average crystallite width and length of rhombic TiO₂ estimated from the (101) and (004) diffraction peaks by Scherrer formula are 15 nm and 31 nm, respectively. Compared with the TEM image (Fig. 1e), these two values are very close to those of rhombic TiO₂ NCs (13nm and 30 nm). By using selected area electron diffraction (SAED), the highly crystalline anatase phase of bone-cuboid TiO₂ nanoparticles is also revealed, as shown in Fig. 2b. The rings can be indexed clearly to diffraction from the (101), (004), (200), (105), (211), and (204) planes of anatase.

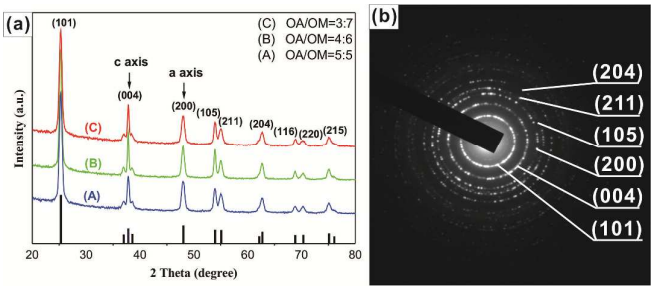


Fig. 2 (a) XRD patterns of the TiO_2 nanoparticles: (A) bone-cuboid; (B) spindle; (C) rhombic. (b) SAED pattern of bone-cuboid TiO_2 nanoparticles.

Organic surfactants take a prominent role in controlling the shape of nanoparticles largely owing to the diversity of organic molecules. We may controll the morphology of TiO_2 nanoparticles by using different capping agents. The selective OA and OM with different binding strengths can act as the surfactants of the anatase TiO_2 {001} face and {101} face, respectively and restrict the growth in corresponding direction. By modulating the OA/OM volume ratio, it is therefore expected that, the shape of TiO_2 NCs can be facile tailored. Interestingly, we also find that the presence of a certain amount of H_2O_2 along with the appropriate oleic acid/oleylamine ratio plays a crucial role in controlling morphology of TiO_2 nanoparticles.

3.2 Synthesis of TiO₂ nanocrystals with different amount of H₂O₂

Fig. 3 shows the corresponding TEM images of the TiO_2 nanoparticles obtained with different amounts of H_2O_2 (here OA/OM=5/5). As shown in Fig. 3a, the formation of TiO_2 nanoparticles undergoes slow nonhydrolytic reaction, which generally produces nanodots or nanorods in the absence of H_2O_2 with poorly crystalline. As trace H_2O_2 was added, the short TiO_2 nanorods with uniform size were obtained (Fig. 3b), indicating the evolution along the [001] direction. Slow hydrolysis of titanium precursors is favorable for forming TiO_2 nanoparticles with controllable shape. With the increasing of

the amount of H_2O_2 (Fig. 3c), the samples became short along [001] direction which is similar to that of the bone-cuboid TiO_2 NCs. Hydrolytic and nonhydrolytic processes reach the equilibrium with a certain range of H_2O_2 . In this case, OA/OM ratio plays a crucial role in controlling the size and shape of TiO_2 nanoparticles. When adding 0.25 ml H_2O_2 into solution, the shape of TiO_2 nanoparticles is close to spherical nanoparticles. Fig. 3d indicates that, adding a large amount of H_2O_2 , titanium butoxide reacts vigorously with water and greatly accelerates the hydrolysis-condensation process. This process thus weakens the stabilizing effect of OA and OM, leading to a decreased anisotropic growth of the products.

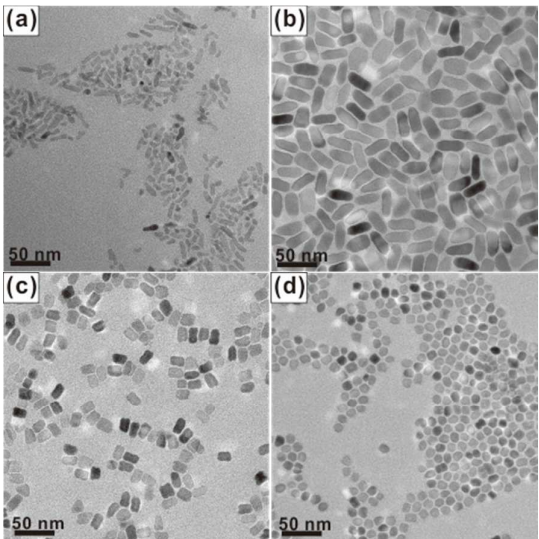


Fig. 3 The TEM images of TiO_2 nanoparticles obtained with different amount of H_2O_2 (here OA/OM=5/5): (a) 0 ml, (b) 0.05 ml, (c) 0.15 ml, (d) 0.25 ml.

In this system, titanium butoxide (TB) can easily react with H₂O₂ to produce interim precursor and hydroxyalkoxide species at high temperature by hydrolysis process. This precursor then reacts with OA to form carboxyalkoxide or with other hydroxyalkoxides as a function of the amount of H₂O₂ and OA used. Subsequently, the reaction between these precursors by a hydrolytic condensation or a nonhydrolytic condensation process forms a Ti-O-Ti network by means of oxolation or olation. OA and OM both act as organic capping agents, controlling the condensation rate without changing the hydrolysis rate.³³ OA can react with TB to generate carboxyalkoxide species and these intermediate products can slow down the hydrolytic condensation process. OM can accelerate the nonhydrolytic condensation process though aminolysis reaction with titanium carboxylalkoxide.34 Hydrolytic process is fast at the initial stage, while the nonhydrolytic process is relatively slow and predominant as the reaction continued. The rate of these two processes is determine by the amount of H₂O₂ and dramatically affects the morphology of the final products. Therefore, TiO₂ nanoparticles with different shapes and sizes have been successfully achieved by varying the amount of H₂O₂. We selected H₂O₂ both as hydrolysis agent and morphology ARTICLE Journal Name

control agent. It not only can simplify the experimental process and shorten the reaction time (12 h) for reducing energy consumption, but also can obtain the highly crystalline titania nanocrystals with good dispersion and homogeneity. As an environmentally friendly shape-controlling agent, $\rm H_2O_2$ may potentially be used to tailor other morphology and facet-controllable nanomaterials. Compare with nanodots, short nanorods and nanospheres, $\rm TiO_2$ NCs (bone-cuboid, spindle and rhombic) have uniform size and shape, and we select them as building blocks to form ordered superlattices.

3.3 Self-assembly of TiO₂ nanocrystals into superlattices

To investigate the shape-directed packing behaviour of ${\rm TiO_2}$ NCs, 2D superlattices of anisotropic ${\rm TiO_2}$ NCs were obtained through slow evaporation of the hexane on the surface of ethylene glycol (EG). The viscous polar EG subphase provided individual NCs of sufficient mobility, even at high nanoparticle volume fractions, to remove defects and access thermodynamically stable assemblies over large areas. In this work, we accumulated three shapes of ${\rm TiO_2}$ NCs into horizontal and vertical 2D superstructures respectively. The assembled arrays could be controlled by adjusting the amount of ${\rm TiO_2}$ NCs and the amount of OA, which both served as surfactants and depletion agents. To the best of our knowledge, these results are the first to be reported for ${\rm TiO_2}$ NCs.

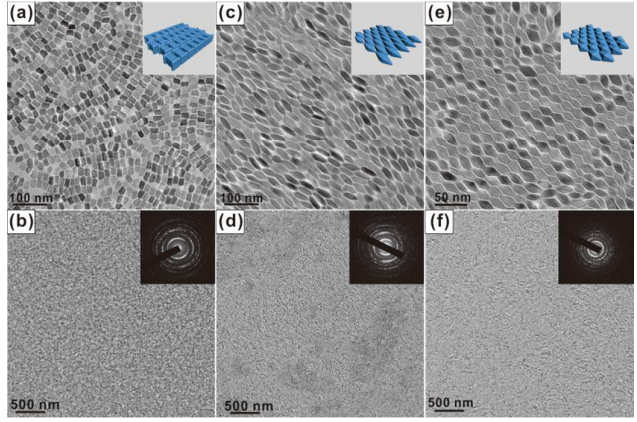


Fig. 4 TEM images of 2D superlattices self-assembled from TiO_2 NCs (200 μ l, 5 μ l). (a) (b) horizontal arrays of bone-cuboid TiO_2 NCs, (c) (d) horizontal arrays of spindle TiO_2 NCs, (e) (f) horizontal arrays of rhombic TiO_2 NCs, Insets show corresponding schematic illustrations and SAED patterns.

The TEM images (Fig. 4) reveal that bone-cuboid, spindle, rhombic ${\rm TiO_2}$ NCs all yielded horizontal self-assembled arrays with low amount of ${\rm TiO_2}$ NCs solution and OA (200 ${\rm \mu l}$, 5 ${\rm \mu l}$). These superlattices in horizontal linear chains are displaced by a part of unit. It is difficult to assemble the bone-cuboid ${\rm TiO_2}$ NCs into highly ordered chain pattern because of theirs uneven (001) faces (Fig. 4a). They tend to be aligned in the [100] direction when rectangular faces are attached. However, Fig. 4c and Fig. 4e show that the spindle and rhombic ${\rm TiO_2}$ NCs can self-assembled into a tight tip-to-tip chain pattern along the [001] direction by elimination of high energy (001)

surfaces. When adding more TiO_2 NCs and OA (400 μ l, 10 μ l) onto EG surface, we can see that TiO_2 NCs dramatically self-organized into vertical 2D superlattices (Fig. 5). These NCs are all oriented in the same direction-one tip of the NCs pointing upward, while the other tip adhered to the liquid-air interface. These assembled architectures exhibit simultaneous orientational and positional order, as indicated by SAED patterns that arises from the periodic atomic lattice planes (Fig. 4 and Fig. 5 insets). The horizontal arrays display highly ordered chain pattern in one-dimension, and the vertically aligned superstructures exhibits ordered arrays in two dimensions with tetragonal symmetry. Moreover, some defects and stacking faults are seen, which do not altered the total packing pattern. Micrometer scale superlattices were achieved in all cases (Fig. 4 and Fig. 5).

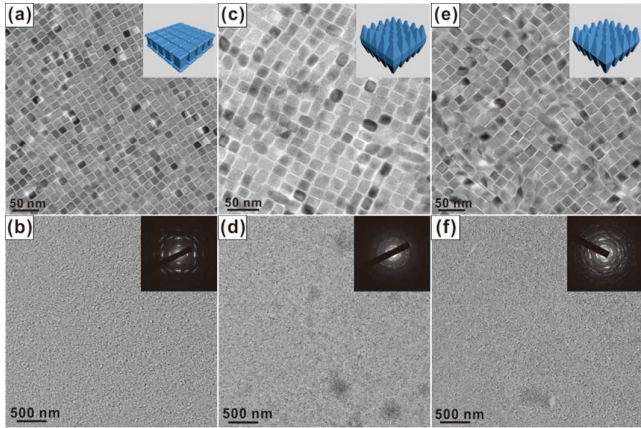


Fig. 5 TEM images of 2D superlattices self-assembled from TiO_2 NCs (400 μ l, 10 μ l). (a) (b) vertical arrays of bone-cuboid TiO_2 NCs, (c) (d) vertical arrays of spindle TiO_2 NCs, (e) (f) vertical arrays of rhombic TiO_2 NCs, Insets show corresponding schematic illustrations and SAED patterns.

In accordance with Onsager's mechanism³⁵ and typical packing configurations in our experiment, we investigated several parameters affecting the assembly formation, including concentration and depletion force, and tried to reveal the underlying mechanisms about how to reproduce highly ordered superlattices in certain configurations. We also discussed the relationship between the shape and the resulting superlattice.

The concentration of colloidal TiO_2 NCs and OA molecules in the spreading solution play a key role in determining the morphologies of 2D superstructures. With a slow solvent evaporation in our experiment, the volume of solvent may diminish after the majority has been evaporated, and the concentration of the NCs increases gradually and the free volume available for each NC decreases. A thin layer of hexane on top of the EG solubilizes the NCs before the hexane evaporates completely. When the thickness of the hexane layer becomes comparable to the largest dimension of an individual NC, clusters will be formed on the surface of the remaining solution as the nucleation sites and then the remained TiO_2 NCs might find their preferred location on the

Journal Name ARTICLE

clusters faces and follow the pattern templated by the underlying structure. This may account for why a certain superstructure type could always maintain its continuity even across a relatively large area. At low nanoparticle and OA concentration (200 µl, 5 µl), chain patterns appear because they have enough space to form horizontal or interleaved arrangements which are favoured to minimize the overall surface energy. When the (400 µl, 10 µl) solution are used, vertical patterns are obtained by maximization of the packing density. With further increase of TiO₂ NCs concentration (600 μ l, 10 μ l), bilayer arrangements are obtained, as depicted in Fig. 6a, 6b and 6c. The bottom-layers in these images are all well-aligned vertical arrays, and the top-layers are mixtures of standing nanoparticles and lying nanoparticles which are not favourable for self-organized superlattices. Particularly, for rhombic TiO2 NCs, we can only obtain disordered top-layers, which may be due to the poor stability of rhombic nanoparticles with upright position. The assembly process is compressing the solution system from the isotropic fluid phase to the anisotropic orderly solid phase, thereby leading to a close-packed ordered arrays. 36-37 Because of different volume fraction of the nanoparticles, we obtained horizontal and vertical ordered superlattices respectively.

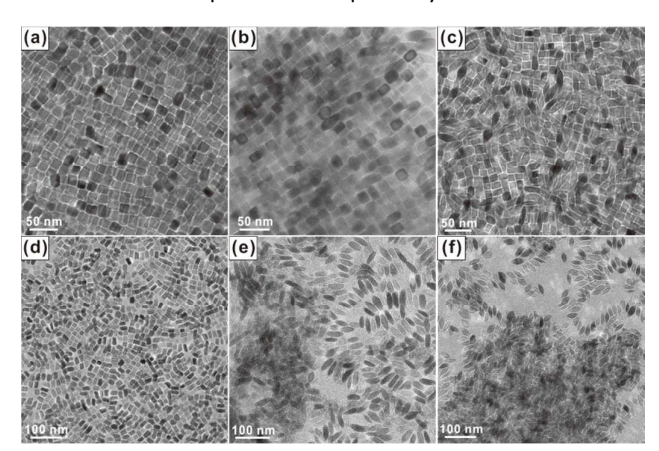


Fig. 6 TEM images of arrangements of self-assembled TiO_2 NCs. (a), (b) and (c) correspond to bone-cuboid, spindle and rhombic TiO_2 NCs with bilayer arrangements (600 μ l, 10 μ l), respectively. (d), (e) and (f) correspond to bone-cuboid, spindle and rhombic TiO_2 NCs with disordered arrangements (200 μ l, 0 μ l), respectively.

Various types of interparticle interactions could be exploited for the assembly, among which depletion attraction stands out. $^{38-39}$ We added a certain amount of OA to the solution of TiO $_2$ NCs and the nonadsorbing OA molecules could behave similarly to polymer molecules. These molecules are usually used to induce depletion attractions between colloid nanoparticles. The large TiO $_2$ NCs and small OA molecules (as depletion agents) all have a high solubility in a nonpolar solvent (hexane). The self-assemble of TiO $_2$ NCs induced by entropically depletion may be explained by the following hypothesis. When gradually increase the NC volume fraction up to a solubility threshold by slow solvent evaporation, the

system of the solution would undergo phase transition of TiO₂ NCs to maximize its total entropy. In this system, the average distance between two adjacent TiO₂ NCs becomes shorter with an increasing concentration of OA molecules, and thus the total volume available to the OA molecules increases owing to the excluded volume among the TiO2 NCs. The experimental results indicated that these assemblies are predominantly entropy driven. When OA molecules are excluded from adjacent nanoparticles, the total entropy of this systems increased. The TiO₂ NCs need to find the proper locations on the growing superlattice to minimize the entropy and form the most ordered structure and the "free" volume available to depletants became maximal to increase the total entropy. As a result, there gives rise to a mean force equivalent to a net osmotic pressure of the small molecules acting to push the large TiO₂ NCs together. The magnitude of the depletion attraction force relies on the OA concentration, the length of carbon chain and molecular weight. When 5 µl OA added, the OA molecules adhere on the surfaces of TiO2 NCs, and draw neighboring NCs together into ordered horizontal 2D superlattices over large areas. At a higher concentration of OA (10 µl), excess OA molecular diffuse in a uniform solution, the entropically depletion-induced assembly of TiO2 NCs can be assembled into vertical 2D monolayers of close-packed tetragonally arrays. The capping ligands of TiO2 NCs are mainly OA, with which three types of TiO2 NCs are synthesized with the OA/OM ratio at 5/5, 4/6 and 3/7, respectively. With the decrease of OA and the increase of OM, the stability of nanoparticles becomes worse in hexane. OA are employed both as surfactants to stable anisotropic nanoparticles and as depletion agents to fabricate ordered superstructures in our experiments. If we ignored the role of depletion interactions without adding OA to the TiO₂ NCs solutions in self-assembly process, then there was only very disordered and agglomerate TiO₂ NCs on the surface of EG, even if other relevant factors were held constant (Fig. 6d, 6e and 6f).

It should be noted that the tips of the spindle and rhombic NCs are slightly truncated. It is very common for colloidal nanoparticles to have tip truncation, as tip truncation minimizes the overall free-energy of nanoparticles. 40 There are two possible equilibrium configurations, in which the TiO $_2$ NCs align their the [001] direction either horizontal or perpendicularly adhered to the liquid–air interface (Fig. 4 and Fig. 5 insets). The truncated TiO $_2$ NCs have multiple options for interfacial adhesion, and have enough time to translate and rotate into ordered arrays in the plane of the air-hexane interface under the assembly process. In particular, we obtained different 2D superlattices from TiO $_2$ NCs over large areas. These TiO $_2$ NCs superlattices may have very importance for exploring new inorganic liquid crystal materials or tailoring novel promising structures for photovoltaic application.

4 Conclusions

In conclusion, a simple solvothermal method has been used to fabricate the TiO_2 nanoparticles with different shapes. The

ARTICLE Journal Name

key characteristic of our approach is using H₂O₂ as hydrolysis agent and morphology control agent to control the nucleation and growth of the TiO2 nanoparticles. We successfully achieved three shapes of TiO2 NCs (bone-cuboid, spindle, rhombic) by varying the OA/OM ratio. All of these TiO₂ NCs can be self-assembled into horizontal and vertical 2D superlattices by controlling the amount of TiO₂ NCs solution and OA at the liquid-air interface. In this system, OA not only act as surfactants to stable anisotropic nanoparticles, but also as depletion agents to induce ordered superlattices. The selforganization process is primarily driven by maximization of the packing density and tuning entropic depletion attraction forces. We also found that TiO₂ NCs with a small truncation can align their [001] direction either horizontal or vertically adhered to the interface, and finally form different arrays. Moreover, we also obtained TiO₂ nanoparticles with different shapes such as nanodots, nanorods and nanospheres by controlling the amount of H2O2. These ordered 2D superlattices provided here will be hopefully used to tailor novel promising structures for wide ranging devices.

Acknowledgements

We are very appreciated for the support from Tie Wang and his group (Institute of Chemistry, The Chinese Academy of Sciences) and Beijing city-level key disciplines and specialties in condensed matter physics (Beihang University).

Notes and references

- G. Liu, H. G. Yang, J. Pan, Y. Q. Yang, G. Q. Lu and H. M. Cheng, Chem. Rev., 2014, 114, 9559–9612.
- Y. Maeda, Y. lizuka and M. Kohyama, J.Am. Chem. Soc., 2013, 135, 906-909.
- L. Etgar, W. Zhang, S. Gabriel, S. G. Hickey, M. K. Nazeeruddin, A. Eychmueller, B. Liu and M. Graetzel, Adv. Mater., 2012, 24, 2202-2206.
- W. D. Zhu, C. W. Wang, J. B. Chen, D. S. Li, F. Zhou and H. L. Zhang, Nanotechnology, 2012, 23, 455204.
- 5 W. J. Zhou, G. J. Du, P. G. Hu, G. H. Li, D. Z. Wang, H. Liu, J. Y. Wang, R. I. Boughton, D. Liu and H. D. Jiang, J. Mater. Chem., 2011. 21, 7937-7945.
- 6 H. G.Yang, C. H. Sun, S. Z. Qiao, J. Zou, G. Liu, S. C. Smith, H. M. Cheng and G. Q. Lu, *Nature*, 2008, 453, 638–641.
- 7 H. Yang, G. Liu, S. Qiao, C. Sun, Y. Jin, S. C. Smith, J. Zou, H. M. Cheng and G. Q. Lu, J. Am. Chem. Soc., 2009, 131, 4078–4083.
- T. R. Gordon, M. Cargnello, T. Paik, F. Mangolini, R. T. Weber, P. Fornasiero and C. B. Murray, J. Am. Chem. Soc., 2012, 134, 6751-6761.
- N. Wu, J. Wang, D. N. Tafen, H. Wang, J.-G. Zheng, J. P. Lewis,
 X. Liu, S. S. Leonard and A. Manivannan, J. Am. Chem. Soc.,
 2010, 132, 6679-6685.
- R. Menzel, A. Duerrbeck, E. Liberti, H. C.Yau, D. McComb and M. S. P. Shaffer, *Chem. Mater.*, 2013, 25, 2137-2145.
- 11 M. Cargnello, T. R. Gordon and C. B. Murray. Chem. Rev., 2014, 114, 9319–9345.
- 12 L. C. Liu, X. R. Gu, Z. Y. Ji, W. X. Zou, C. J. Tang, F. Gao and L. Dong, *J. Phys. Chem. C.*, 2013, **117**, 18578–18587.
- 13 T. Y. Li, B. Z. Tian, J. L. Zhang, R. F. Dong, T. T. Wang and F. Yang, *Ind. Eng. Chem. Res.*, 2013, 52, 6704–6712.

- 14 X. W. Zhao, W. Z. Jin, J. G. Cai, J. F. Ye, Z. H. Li, Y. R. Ma, J. L. Xie and L. M. Qi, Adv. Funct. Mater., 2011, 21, 3554–3563.
- 15 C. Chen, R. Hu, K. G. Mai, Z. M. Ren, H. Wang, G. D. Qian and Z. Y. Wang, *Cryst. Growth Des.*, 2011, **11**, 5221–5226.
- 16 D. V. Talapin, J. Lee, M. V. Kovalenko and E. V. Shevchenko, Chem. Rev., 2010, 110, 389–458.
- 17 E. Talgorn, Y. Gao, M. Aerts, L. T. Kunneman, J. M. Schins, T. J. Sevenije, M. A. van Huis, H. S. J. van der Zant, A. J. Houtepen and L. D. A. Siebbeles, *Nat. Nanotechnol.*, 2011, 6, 733–739.
- 18 J.Tang, K. W. Kemp, S. Hoogland, K. S. Jeong, H. Liu, L. Levina, M. Furukawa, X. Wang, R. Debnath, D. Cha, K. W. Chou, A. Fischer, A. Amassian, J. B. Asbury and E. H. Sargent, *Nat. Mater.*, 2011, **10**, 765–771.
- 19 D. Vanmaekelbergh, Nano Today, 2011, **6**, 419–437.
- 20 Y. Shirasaki, G. J. Supran, M. G. Bawendi, V. Bulović, *Nat. Photonics.*, 2013, **7**, 13–23.
- 21 Z. Nie, A. Petukhova and E. Kumacheva, *Nat. Nanotechnol.*, 2010, **5**, 15–25.
- 22 R. Y. Wang, J. P. Feser, J.-S. Lee, D. V. Talapin, R. Segalman and A. Majumdar, *Nano Lett.*, 2008, **8**, 2283–2288.
- 23 Y. Kang, X. Ye, J. Chen, L. Qi, R. E. Diaz, V. Doan-Nguyen, G. Xing, C. R. Kagan, J. Li, R. J. Gorte, E. A. Stach and C. B. Murray, J. Am. Chem. Soc., 2013, 135, 1499–1505.
- 24 Y. Nakagawa, H. Kageyama, Y. Oaki and H. Imai. *J. Am. Chem. Soc.*, 2014, **136**, 3716–3719.
- 25 X. C. Ye, J. A. Millan, M. Engel, J. Chen, B. T. Diroll, S. C. Glotzer and C. B. Murray. *Nano Lett.*, 2013, 13, 4980–4988.
- 26 M. A. Boles and D. V. Talapin. J. Am. Chem. Soc., 2014, 136, 5868–5871.
- 27 B. Ye, G. Qian, X. Fan and Z. Wang, Current. Nanoscience, 2010, 6, 262-268.
- 28 C. T. Dinh, T. D. Nguyen, F. Kleitz and T. O. Do, ACS Nano, 2009, 3, 3737-3743.
- J. Chen, A. Dong, J. Cai, X. Ye, Y. Kang, J. M. Kikkawa and C. B. Murray, *Nano Lett.*, 2010, **10**, 5103–5108.
- 30 A. S. Barnard and L. A. Curtiss, *Nano Lett.*, 2005, **5**, 1261–1266.
- 31 J. Y. Kim, S. B. Choi, D. W. Kim, S. Lee, H. S. Jung, J.-K. Lee and K. S. Hong, *Langmuir*, 2008, **24**, 4316-4319.
- 32 R. Buonsanti, E. Carlino, C. Giannini, D. Altamura, L. De Marco, R. Giannuzzi, M. Manca, G. Gigli and P. D. Cozzoli, J. Am. Chem. Soc., 2011, 133, 19216-19239.
- 33 Y. Murakami, T. Matsumoto and Y. Takasu, *J. Phys. Chem. B.*, 1999, **103**, 1836–1840.
- 34 Z. Zhang, X. Zhong, S. Liu, D. Li and M. Han, *Angew. Chem., Int. Ed.,* 2005, **44**, 3466–3470.
- 35 L. Onsager, Ann. N. Y. Acad. Sci., 1949, **51**, 627-659.
- 36 W. V. D. Stam, A. P. Gantapara, Q. A. Akkerman, G. Soligno, J. D. Meeldijk, R. V. Roij, M. Dijkstra and C. D. M. Donega, *Nano Lett.*, 2014, 14, 1032–1037
- 37 X. C. Ye, J. Chen, S. C. Glotzer and C. B. Murray. *Nature chemistry*, 2013, 5, 466-473.
- 38 D. Baranov, A. Fiore, M. V. Huis, C. Giannini, A. Falqui, U. Lafont, H. Zandbergen, M. Zanella, R. Cingolani and L. Manna. *Nano Lett.*, 2010, 10, 743-749.
- 39 J. Zhang, P. R. Lang, M. Meyer and J.K. G. Dhont, *Langmuir*, 2013, **29**, 4679–4687.
- 40 C. D. M. Donega, Chem. Soc. Rev., 2011, 40, 1512-1546.